

FABRICATION OF NANOSTRUCTURED IRON AND ZINC PARTICLES BY *DIOSPYROS CHLOROXYLON* (ROXB.) LEAF EXTRACT: CHARACTERIZATION, ADSORPTION MODELING AND CARCINOGENIC DYE ADSORPTION APPLICATIONS

CHANDANA NARASIMHA RAO , M. SUJATHA* 

Department of Chemistry, Koneru Lakshmaiah Education Foundation, Vaddeswaram, Guntur-522502, A. P. India

*Corresponding author: M. Sujatha; *Email: sujathaenviero@kluniversity.in

Received: 10 Sep 2023, Revised and Accepted: 28 Oct 2023

ABSTRACT

Objective: The discharge of these synthetic food dyes, such as sunset yellow and tartrazine, into industrial wastewater can lead to significant environmental and health issues. Its removal through effective adsorption presents an economical and efficient solution. Hence this study proposed to fabricate metal nanoparticles for the adsorption of carcinogenic dyes.

Methods: The fabrication of iron and zinc nanoparticles employed the green synthesis methodology, utilizing an aqueous extract of *Diospyros chloroxylon* (Roxb.) as a reducing agent. The fabricated nanoparticles were characterized using TEM (Transmission Electron Microscopy), EDX (Energy-Dispersive X-ray Spectroscopy), SEM (Scanning Electron Microscopy), FTIR (Fourier-Transform Infrared Spectroscopy), and UV-Visible Spectroscopy. The nanoparticles were studied for its efficiency for the adsorption of carcinogenic dyes such as tartrazine and Sunset Yellow.

Results: The iron nanoparticles were noticed to be uniformly distributed rod-shaped particles having smooth surfaces with 23-51 nm size range and an average particle size of 34 nm. Whereas the iron nanoparticles were noticed to be uniformly distributed spherical to oval shape with 35 nm to 68 nm size range and an average particle size 53 nm. The XRD results confirm that the iron nanoparticles were rhombohedral phase structure with 71.91 % of elemental iron whereas the zinc nanoparticles were noticed to be hexagonal Wurtzite phase structure having 69.4 % of metallic zinc. These synthesized nanoparticles were applied for the removal of sunset yellow and tartrazine dyes were investigated and found more than 90 % was removed. Adsorption isotherm study was best fitted with Langmuir model, and the maximal adsorption capacity was found to be 52.18 and 75.04 mg/g for sunset yellow using iron and zinc nanoparticles, whereas tartrazine maximum adsorption capacity was noticed to be 69.96 and 84.24 mg/g for iron and zinc nanoparticles. The adsorption reaction follows pseudo-first-order kinetics with high correlation coefficient. Repeated cycles of regeneration, reuse and stability showed very high removal efficiency and stability.

Conclusion: The biosynthesis of metal nanoparticles demonstrates substantial promise for applications in environmental protection.

Keywords: Iron nanoparticles, Zinc nanoparticles, *Diospyros chloroxylon*, Characterisation, Adsorption studies, Carcinogenic dye reduction

© 2024 The Authors. Published by Innovare Academic Sciences Pvt Ltd. This is an open access article under the CC BY license (<https://creativecommons.org/licenses/by/4.0/>)
DOI: <https://dx.doi.org/10.22159/ijap.2024v16i1.49344> Journal homepage: <https://innovareacademics.in/journals/index.php/ijap>

INTRODUCTION

Dyes represent significant contaminants across various industries, including textiles, food production, paper manufacturing, paints, pharmaceuticals, and more. This is a critical concern as, in many instances, these dyes are directly discharged into wastewater, leading to both environmental and aesthetic pollution [1]. Dyes can be categorized into three main groups based on their behavior in aqueous solutions: anionic (including azoic, acid, direct, and reactive dyes), cationic (basic dyes), and nonionic (disperse dyes) [2].

Sunset yellow and tartrazine are prevalent azo dyes frequently incorporated into beverages and food items like soda, fruit juices, confectionery, and cakes. These dyes rank as the second and third most commonly used color additives in numerous beverage products [3]. Notably, they exhibit considerable resistance to factors like light, oxygen, and pH variations, making them an attractive choice for manufacturers. Additionally, they are more cost-effective than natural dyes. However, it is important to note that sunset yellow and tartrazine are associated with potential mutagenic and carcinogenic properties due to the presence of azo groups [4]. In light of this concern, certain northern European countries, including Finland and Norway, have already imposed bans on the use of sunset yellow as a precautionary measure [5].

A majority of the dye species found in textile wastewater are azo dyes, comprising more than half of the total [6]. The treatment of azo dyes presents unique challenges due to the presence of sulfonic acid groups, which render the dyes polar and highly soluble in water. Consequently, traditional methods like adsorption onto activated carbon with nonpolar surfaces are ineffective. Instead, it becomes necessary to focus on the degradation of these dyes and the

subsequent removal of their degradation products, particularly aromatic amines, through adsorption techniques.

Various techniques encompassing physical, chemical, and biological processes have been employed for the remediation of contaminated water [7]. Regrettably, many of these methods suffer from high costs and limited removal efficiency. In particular, when it comes to the removal of industrial dyes, researchers have explored physical and chemical strategies, such as Fenton's reagent, electrochemical processes, adsorption materials, and catalytic reductive approaches [8]. Fenton's reagent stands out as an effective means of decolorizing both soluble and insoluble dyes, although it generates sludge as a byproduct [9]. Electrochemical destruction, while proficient at breaking down dye compounds into nonhazardous forms, is constrained by the elevated cost of electricity [10]. Activated carbon, known for its dye removal capabilities through adsorption, presents the drawback of requiring regeneration, incurring a loss of carbon, and raising overall expenses [11].

More recently, green nanoparticles have gained prominence in water treatment due to its non-toxic, cost-effective, and environmentally friendly nature [12]. The high dye reduction efficiency of nanoparticles was due to its high specific surface area, small particle size, and reactivity [13]. In view of this, this study intended to synthesize iron and zinc nanoparticles utilizing leaf extract of *Diospyros chloroxylon* (Roxb.) as reducing and capping agent. The characterization of *Diospyros chloroxylon* mediated iron and zinc nanoparticles was conducted with different characterization techniques. Further, the synthesised zinc nanoparticles were applied as catalyst for the removal of carcinogenic yellow azo dyes such as sunset yellow and tartrazine in an aqueous solution.

MATERIALS AND METHODS

Collection of plant material

Leaves from the *Diospyros chloroxylon* (Roxb.) plant were gathered within the Addateegala forest, located in the East Godavari district of Andhra Pradesh. The collected plant sample was authenticated at department of Botany, SRR and CVR Government Degree College (A) Vijayawada with plant authentication number SRR-CVR/2022-23/Bot/14. To ensure their cleanliness, the collected leaves underwent a meticulous cleaning process involving the removal of sand and dirt using sterile cotton and subsequent rinsing with distilled water. Afterward, any residual water droplets on the cleaned leaves were carefully removed using tissue paper. The plant material was then finely chopped into small pieces before being gently dried in the shade. Finally, the dried leaf material was carefully stored separately for future use.

Extractions of plant materials

Precisely 10 grams of plant powder were meticulously measured and placed into a 250 ml beaker already containing 100 ml of double-distilled water. The mixture of plant material and water was then subjected to boiling on a hot plate, maintaining a temperature of 40 °C for a duration of 80 min. This process effectively facilitated the extraction of the plant's phytochemical constituents into the aqueous solvent. Following the extraction, the resultant extract underwent filtration, with any remaining plant material settling as sediment and being subsequently discarded. The transparent filtrate, devoid of any particulate matter, was then adjusted to a final volume of 100 ml by adding additional distilled water. This clear filtrate was utilized for the fabrication of nanoparticles [14].

Synthesis of zinc nanoparticles

The aqueous leaf extract and zinc acetate solution in 10:90 (v/v) was mixed and the homogenous mixture was prepared by stirring the solution in a magnetic stirrer for 4 h without heating. Then 20 ml of ethanolic sodium hydroxide solution was added and stirred for 5 min. The precipitate at the bottom of the flask was collected by removing the excess mother liquid and then obtained precipitate washed with excess distilled water to remove the extract particles on the precipitate [15]. Then the precipitate was purified by heating at 300 °C for 45 min in a muffle furnace. The obtained particles were preserved for further study.

Fabrication of iron nanoparticles

The aqueous extract was prepared by heating 100 g/l leaves until boiling and continued for 1 h at 50 °C. After settling, the extract was filter through whatman filter paper (No 1 grade) with a vacuum filtration kit. In a separate volumetric flask, aqueous leaf extract and 0.10 M metal precursor solution (19.9 g of FeCl₂·3H₂O in 1L water) were mixed in 6:4 (v/v) and 8:2 (v/v). In continuation, the pH of the mixture was bring to 6.0 using an aqueous NaOH (1.0 M) solution. The nanoparticles formed in the reaction mixture were collected by centrifugation followed by heating in a hot plate and then by drying in a fume hood [16, 17].

Characterization

The synthesized zinc nanoparticles underwent a comprehensive characterization using a suite of analytical techniques, including TEM, EDX, SEM, FTIR, and UV-visible spectroscopy. The initial formation of nanoparticles was noted through a noticeable colour change during the initial reaction. This change in colour was further confirmed using UV-Visible Spectral Analysis, which was carried out using the Double Bean UV-Visible Spectrophotometer from JASCO (Japan) and scanning across the 800–300 nm range. FTIR analysis was conducted on a Bruker (USA) instrument, covering the spectral range of 500-4000 cm⁻¹. This analysis aimed to identify the phytochemical groups responsible for nanoparticle formation. TEM analysis was conducted using the Jeol JEM 2100 instrument from Japan, operating at 120 keV. Before analysis, the nanoparticles underwent a thorough methanol wash and were then mounted on copper grids coated with carbon. For SEM analysis and elemental composition evaluation, the Jeol 6390LA SEM instrument, coupled with OXFORD XMX-N EDX, was employed. The instrument, utilizing a

Tungsten lamp, operated at an accelerating voltage ranging from 0.5 to 30 kV. The nanoparticles were affixed to carbon adhesive tapes and supported on metal disks, with images and elemental composition data recorded at various magnifications. XRD analysis was carried out using the Bruker D8 Advance EDX instrument, operating with an energy resolution of <380 eV at 8 KeV and employing Cu K α radiation as the source. To prevent sodium chloride crystallization, the nanoparticles underwent multiple ethanol washes prior to analysis. Scanning was performed over a 2 θ range of 20-100 degrees.

Adsorption methodology

To initiate the experiments, stock solutions of tartrazine and sunset yellow dyes were prepared at a concentration of 0.5 g/l separately in distilled water. Subsequently, these stock solutions were further diluted to desired concentrations during the experimental study. The absorbance values of both dyes were determined using UV spectrophotometer. The adsorption experiments were conducted at room temperature and were carried out using an automatic shaker to ensure consistent reactions. Various experimental parameters, including dosage, contact time, initial dye concentration, pH levels, the presence of interfering salts, and variations in temperature was varied. In each experiment performed, the adsorption capacity equilibrium (q_e) and metal removal (R in %) which were calculated for both nanoparticles using formula:

$$q_e = \frac{C_i - C_e \times V}{m} \text{----- eq. 1}$$

$$R (\%) = \frac{C_i - C_e \times V}{C_i} \times 100 \text{----- eq. 2}$$

Where C_i = metal ion initial concentration; C_e = metal ion equilibrium concentration; V = volume of metal solution in L and m = weight of nanoparticles taken as adsorbent.

Adsorption kinetic studies

The investigation of adsorption kinetics stands as a pivotal aspect in the rational design of industrial adsorption processes. The dye reduction efficiency kinetics of synthesised nanoparticles was conducted in a series of experiments conducted within 250 ml Erlenmeyer flasks. Each flask contained 0.2 grams (equivalent to 2 g/l) of nanoparticles, combined with a 100 ml dye suspension containing dyes at their respective required concentrations, all adjusted to their optimum pH and temperature conditions.

These suspensions were maintained at a constant temperature of 30±0.2 °C while being agitated at 200 rpm using a shaker. Samples were collected at various time intervals until equilibrium was reached. Subsequently, these samples were subjected to analysis, and the percentage removal of dye or metals was determined utilizing Equation (2).

To gain insights into the dynamics of dye adsorption by synthesized nanoparticles, we conducted a kinetic study employing both the Lagergren pseudo-first-order and chemisorption's pseudo-second-order kinetics models. The Lagergren pseudo-first-order equation as follows:

$$(q_e - qt) = \ln q_e - K_1 t \text{----- eq. 3}$$

This equation served as a basis for the evaluation of the adsorption kinetics. In the equation qt (mg/g⁻¹) represents the adsorption capacity of at a given time 't' and q_e (mg/g) is the adsorption capacity at equilibrium (mg/g), K_1 (min⁻¹) stands for the pseudo-first-order rate constant.

The pseudo-second-order kinetic model can be expressed in its linear form as follows:

$$t/q_t = 1/K_2 q_e^2 + t/q_e \text{----- eq. 4}$$

Where K_2 represents the pseudo-second-order rate constant in g mg⁻¹ min⁻¹.

Adsorption isothermal study

The equilibrium concentrations, along with their corresponding adsorption efficiency were utilized to construct adsorption

isotherms. These isotherms were generated in the concentration range of 5-100 mg/l for both dyes and experiments were conducted under their respective optimal pH and temperature conditions. All other parameters and sample analyses were carried out in accordance with the previously described methods. The equilibrium concentration of adsorbed metal (q_e) was determined using equation 1.

The adsorption isotherm represents the relationship between the quantity of a substance adsorbed per unit mass of adsorbent at a constant temperature and its concentration in the equilibrium solution. The Langmuir and Freundlich isotherms are the two most commonly utilized models to depict data on adsorption from a solution.

Langmuir isotherm

The Langmuir isotherm is relevant when the adsorption of the adsorbate is constrained to a single layer on the surface of the adsorbent. The linear representation of the Langmuir isotherm is expressed by the following equation:

$$C_e/q_e = 1/K_L \cdot Q_0 + C_e/Q_0 \text{ ----- eq. 5}$$

The potential for the adsorption process can be accessed through the separation factor (R_L), which can be computed using the following equation:

$$R_L = 1/1 + K_L C_0 \text{ ----- eq. 6}$$

Where K_L represents Langmuir constant and C_0 is the concentration of dye solution prepared. R_L indicates the isotherm to be unfavorable ($R_L > 1$), linear ($R_L = 1$), irreversible ($R_L = 0$) or favorable ($0 < R_L < 1$).

Freundlich isotherm

The empirical Freundlich model, which describes adsorption on a heterogeneous surface, is expressed by the following equation:

$$q_e = \ln K F + \frac{1}{n} \ln C_e \text{ ----- eq. 7}$$

Where K_F represents Freundlich constants related expressed in mg/g and n represents adsorption favorability

Stability and recyclability of nanoparticles

The stability of synthesized nanoparticles was evaluated chemically by mixing 0.1 g of synthesized nanoparticles with 200 ml of aqueous solution at wide pH range i. e from 2.0 to 10. Then the reaction mixture was kept in an orbital shaker for 24 h at 75 °C. The zinc ions dissolved in the solution was evaluated using atomic absorption spectrophotometer.

The recyclability of the synthesized nanoparticles plays a significant role as the particles were recyclable, it will reduce the experimental cost. The nanoparticles, after completion of metal reduction study, were washed with 0.01 M hydrochloric acid EDTA separately and then washed several times with distilled water. The particles were dried 24 h at 60 °C and then were utilized for adsorption study and the same procedure was repeated for 5 times and based on the results, the reusability was evaluated.

RESULTS AND DISCUSSION

During the nanoparticle synthesis process, a striking transformation in the color of the leaf extract was observed due to the reaction with the metal solution. The observed color change was further quantified instrumentally using a spectrophotometer across the wavelength range of 800-300 nm, whereas the absorption spectra of the aqueous leaf extract was measured within the scan range of 800-200 nm.

Notably, the UV scanning spectra of the synthesized iron and zinc nanoparticles exhibited highly intense absorption maxima at 567 nm and 381 nm, respectively, suggest the formation of nanoparticles. The UV absorption maxima noticed for the synthesized iron and zinc nanoparticles was well correlated with the findings reported in literature [18-22]. These spectral changes strongly suggest the active involvement of biomolecules within the leaf extract of *D chloroxylon* in the process of nanoparticle formation.

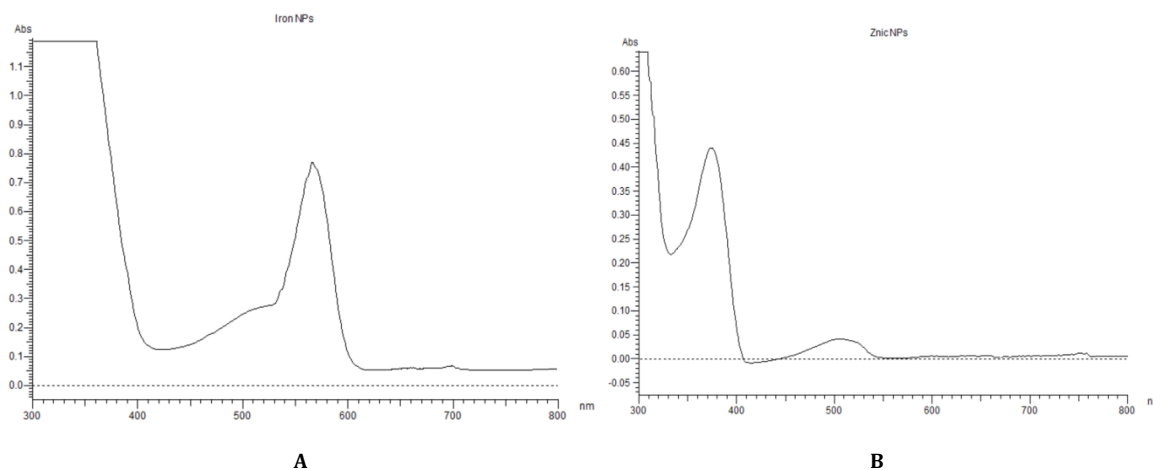
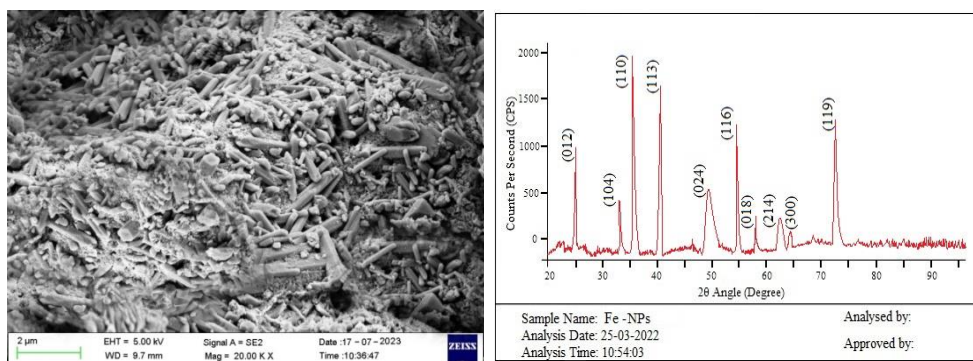


Fig. 1: UV-visible absorption spectra of iron (A) and zinc (B) nanoparticles synthesised using aqueous leaf extract of *D chloroxylon*

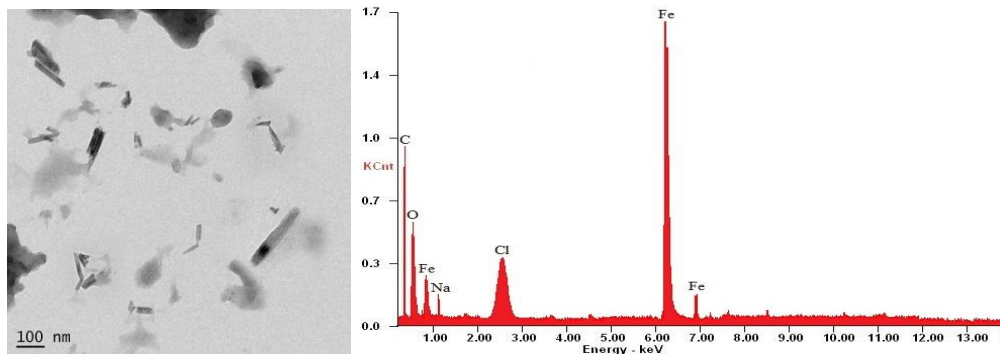
The involvement of various bioactive chemical constituents during the fabrication of nanoparticles was confirmed by FTIR analysis. The FTIR results confirm the presence of plant-based functional groups such as flavonoids, phenolic compounds and alkaloids that are actively involved in the formation of both iron and zinc nanoparticles. The SEM analysis both iron and zinc nanoparticles was performed to evaluate the surface morphology. The iron nanoparticles were noticed to be uniformly distributed rod-shaped particles having smooth surfaces with 23-51 nm size range and an average particle size of 34 nm. Whereas the iron nanoparticles were noticed to be uniformly distributed spherical to oval shape with 35 nm to 68 nm size range and an average particle size 53 nm. The XRD

results confirm that the iron nanoparticles were rhombohedral phase structure with the correlation of standard JCPDS card no 33-0664 whereas the zinc nanoparticle were noticed to be hexagonal Wurtzite phase structure of the particles in correlation with the standard JCPDS card no 89-0510. The crystal structure was in correlation with the findings reported in literature [23, 24]. The elemental analysis using EDX suggest that the iron nanoparticles contains 71.91 % of elemental iron whereas the zinc nanoparticles were noticed to be having 69.4 % of the metallic zinc. Based on various characterization studies, it was confirmed that the synthesized iron and zinc particles were in nano size with high purity. The characterization results were presented in fig. 2 and 3 for iron and zinc nanoparticles, respectively.



A) SEM

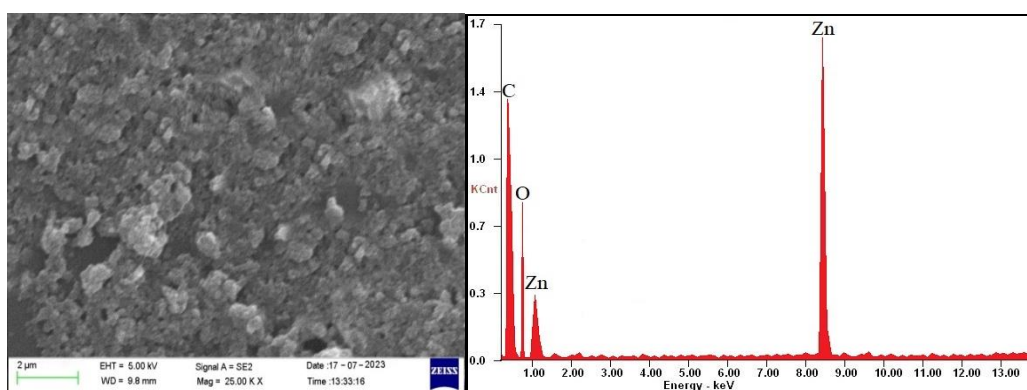
B) XRD



C) TEM

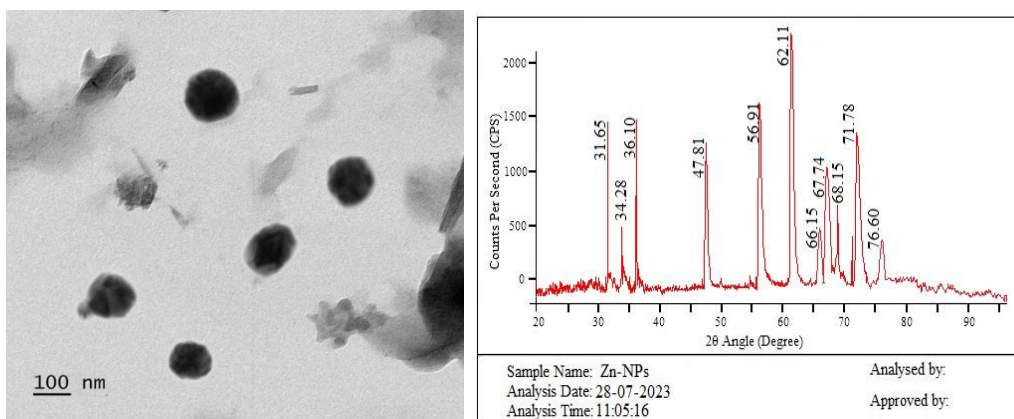
D) EDX

Fig. 2: Structural characterization of synthesized iron nanoparticles



A) SEM

B) EDX



C) TEM

D) XRD

Fig. 3: Structural characterization of synthesized zinc nanoparticles

Adsorption study

The dye adsorption efficiency of the synthesized iron and zinc nanoparticles were evaluated by optimizing various experimental conditions such as concentration of dye, dose of adsorbent, time of adsorption, pH of solution and agitation rate. All the experiments were performed in triplicate and results were presented as mean \pm standard deviation.

The pH influence on the adsorption of sunset yellow and tartrazine by synthesized nanoparticles was assessed in 2-8 pH ranges. The maximum contact time of 120 min, average reaction mixture agitation rate of 100 rpm with 0.5 g/l of adsorbent dose was studied for optimization of pH of the reaction mixture. Based on results as shown in fig. 4A, it was observed that, on increase in the pH of the reaction mixture from 2 to 8 the removal efficiency was increased till neutral pH i. e 7 and then decreased at pH 8 for both dyes using both iron and zinc nanoparticles. The maximum adsorption of sunset yellow was noticed at pH 6 with a % adsorption of 84.46 % using iron nanoparticles and 81.46 \pm 0.36 % at pH 7 using zinc nanoparticles. Whereas tartrazine high % adsorption was noticed at pH 7.0 with 86.79 \pm 0.47 % and 89.19 \pm 0.41 % adsorption at pH 7.0 using synthesized iron and zinc nanoparticles, respectively.

The reaction mixture agitation rate of 25 to 150 rpm was studied for evaluating the dye adsorption efficiency of synthesized nanoparticles. Based on results as shown in fig. 4B, it was observed that the dye removal efficiency of both nanoparticles was very low at a low agitation rate and then goes on to increase with increase in the

agitation rate up to 100 rpm for both dyes. The agitation rate of 125 and 150 rpm, the % adsorption was noticed to be decrease and hence 100 rpm was selected as optimized agitation rate for the adsorption of dyes using synthesized iron and zinc nanoparticles.

The influence of adsorbent dose on adsorption of sunset yellow and tartrazine was studied with a dose of 0.25 to 1.0 g/l under fixed contact time, optimized pH and agitation rate. The relation of adsorbent dose with dye adsorption efficiency was presented in fig. 4C. The maximum adsorption of sunset yellow was noticed with an adsorbent dose of 0.5 and 0.75 g/l with an adsorption efficiency of 76.68 \pm 1.01 % and 79.26 \pm 0.85 %, respectively, using iron and zinc nanoparticles as adsorbent. Whereas the maximum adsorption of tartrazine was noticed with an adsorbent dose of 0.75 and 0.50 g/l with an adsorption efficiency of 86.43 \pm 1.32 % and 73.63 \pm 1.17 %, respectively, using iron and zinc nanoparticles as adsorbent. The outcomes clearly demonstrate that an increase in the adsorbent dosage leads to a proportional enhancement in the removal efficiency of dyes. Beginning at 0.25 g/l with increments of 0.25 g/l, the dosage was progressively increased and results showed a consistent increase in removal efficiency until it reached the optimal dosages. The heightened percentage of adsorption with an increased adsorbent dose can be attributed to the expanded surface area of the adsorbent and the availability of more adsorption sites. However, the rate of adsorption began to decline as the adsorbent dose continued to increase beyond the optimal value. This decline is primarily due to the overlap of adsorption sites, resulting from an overabundance of adsorbent particles.

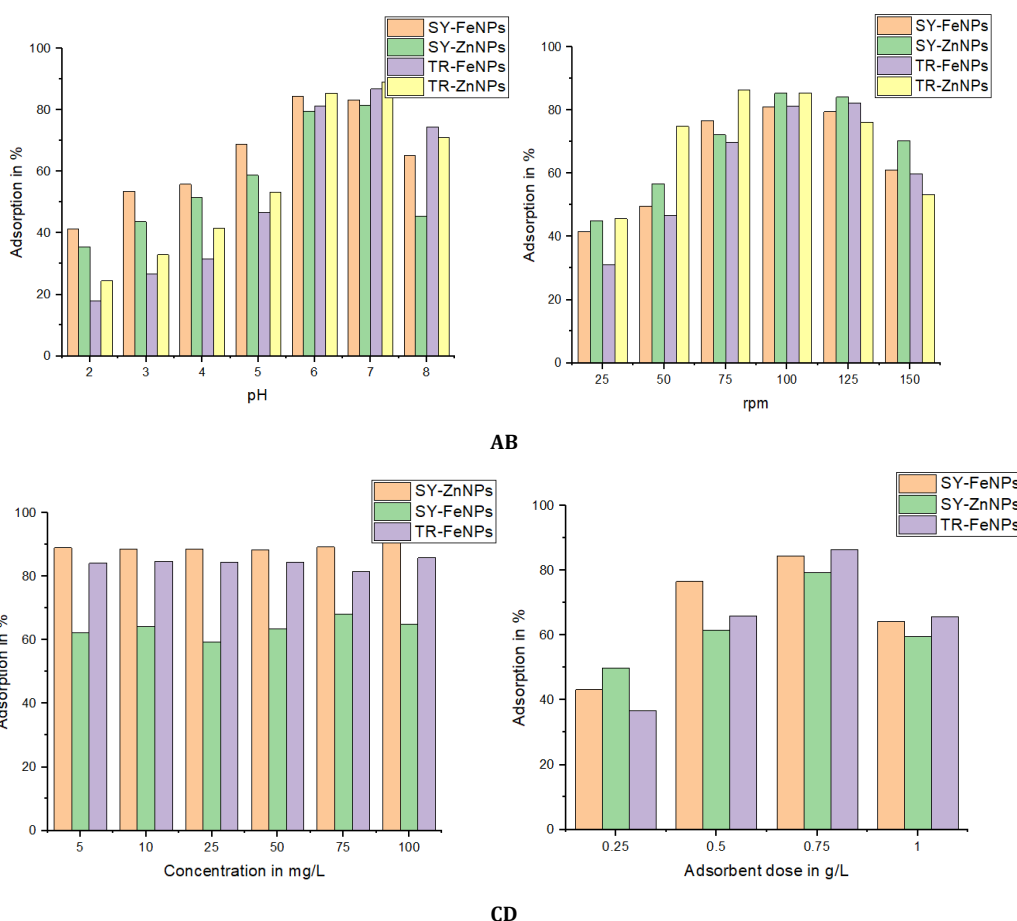


Fig. 4: Optimization of experimental parameters for the adsorption of dyes, A) pH of the reaction mixture; B) agitation rate of the reaction mixture; C) concentration of dye solution; D) dose of nano adsorbent

The optimal time that shows maximum adsorption was evaluated with a range of adsorption time of 15-90 min by maintaining optimized reaction mixture pH, agitation rate, dye strength and dose of nano adsorbent. The quantity of dye adsorbed was evaluated using a UV-visible

spectrophotometer. Fig. 5 displays the UV-visible absorption spectra of dye solutions, encompassing both untreated and nanoparticle-treated samples. The illustration distinctly illustrates a significant decline in dye concentration, signifying a reduction within the aqueous dye solution.

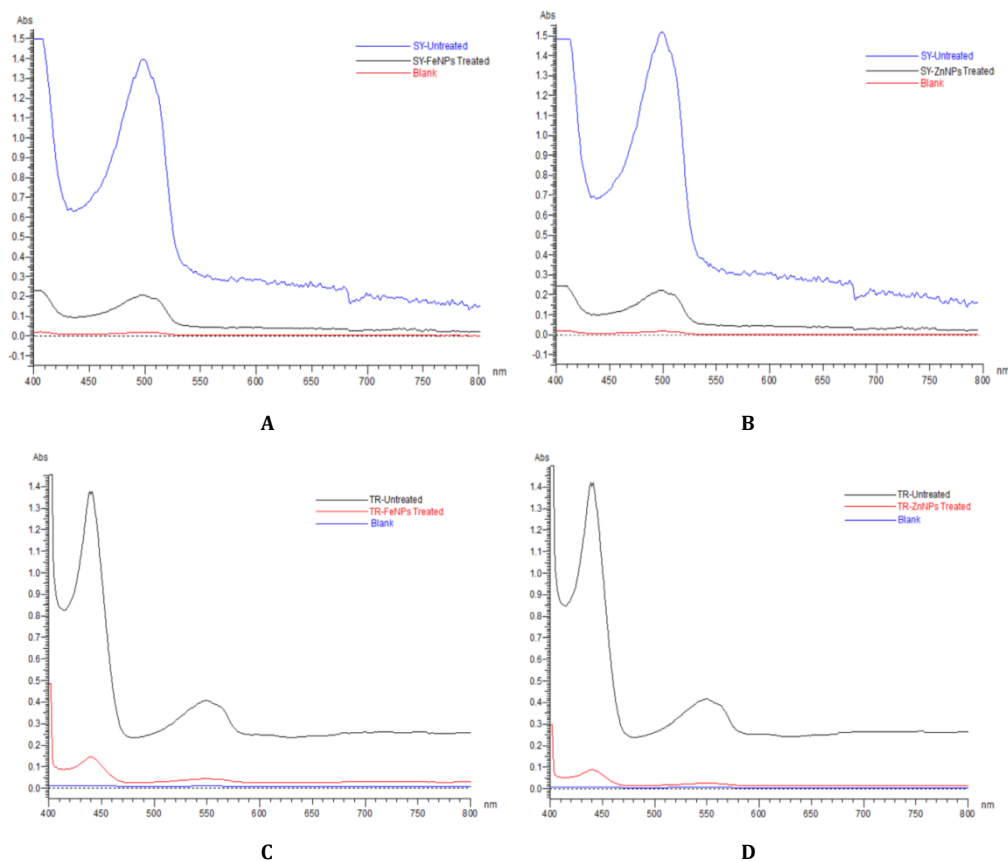


Fig. 5: Overlay UV scanning spectra identified in the dye adsorption study

The contact time versus adsorption of sunset yellow and tartrazine using synthesized iron and zinc nanoparticles was presented in fig. 6. The sunset yellow adsorption was noticed at a % of 67.91 and 84.56 using synthesized iron and zinc nanoparticles as adsorbent respectively with in short period of 45 min. Whereas at this time, the tartrazine adsorption was noticed to be 54.32 % and 69.58 respectively, using iron and zinc nanoparticles as adsorbent. This evidence that the process of dye adsorption initiated with the rapid

adsorption of dye onto the surface of nanoparticles. This initial phase of adsorption gradually decelerates once most of the available active sites become saturated. The adsorption of sunset yellow at 75 min contact time was noticed to be 89.74 % and 91.25 %, whereas tartrazine adsorption was noticed to be 87.34 % and 92.25 %, respectively, using iron and zinc nanoparticles. This study suggests that the nanoparticles possess high adsorption efficiency towards carcinogenic dyes in the study.

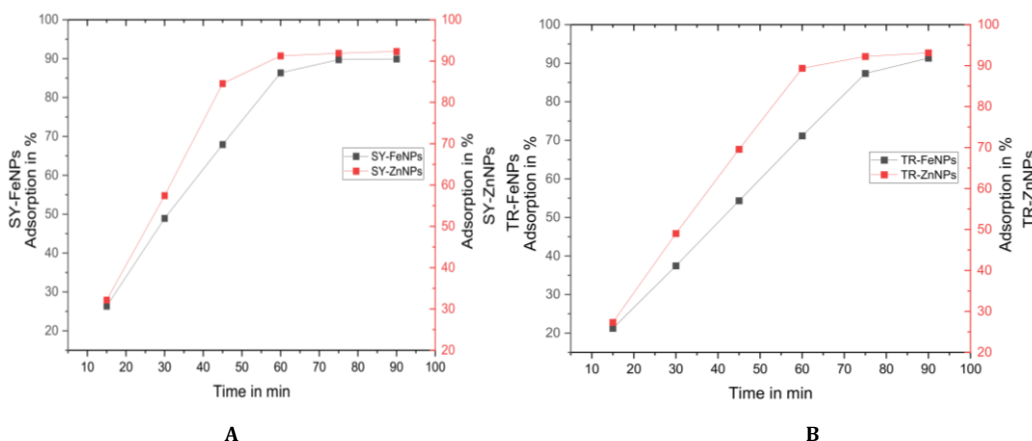


Fig. 6: Results observed during adsorption study of sunset yellow (A) and tartrazine (B) dyes using synthesized nanoparticles

Adsorption isotherm model

We subjected the adsorption data of sunset yellow and tartrazine to fitting with two distinct isotherm models such as Langmuir and Freundlich. This was done to establish a correlation between our experimental findings and these models. The model that provided the best fit to the data exhibited an exceptional correlation

coefficient (R^2) equal to unity. The Langmuir isotherm model posits that adsorption entails a monolayer formation process, wherein each active site accommodates one dye ion, and all these sites are energetically equivalent, with no interaction among adsorbed ions. Our results demonstrated that the experimental data for the adsorption of dye on synthesized iron and zinc nanoparticles exhibited a strong fit with the Langmuir isotherm model.

The correlation coefficient noticed in Langmuir isotherm graph was noticed to be very close to 1 suggesting that the monolayer adsorption was favorable in the study. The q_{\max} (mg/g) was noticed to be very high for the studied dyes suggest that the process shows maximum adsorption efficiency. According to this isotherm, the concentration of ions adhering to the sorbent surface escalates as the adsorbent concentration rises, potentially allowing for the formation of multiple

layers. When the adsorption intensity (n) surpasses one, it signifies the ease of isolating ions from the solution and, consequently, the feasibility of the adsorption process. The isothermal parameters calculated for adsorption study of sunset yellow and tartrazine using synthesized iron and zinc nanoparticles was tabulated in table 1. The Langmuir and Freundlich isotherm graphs for observed in the study were presented in fig. 7 and 8, respectively.

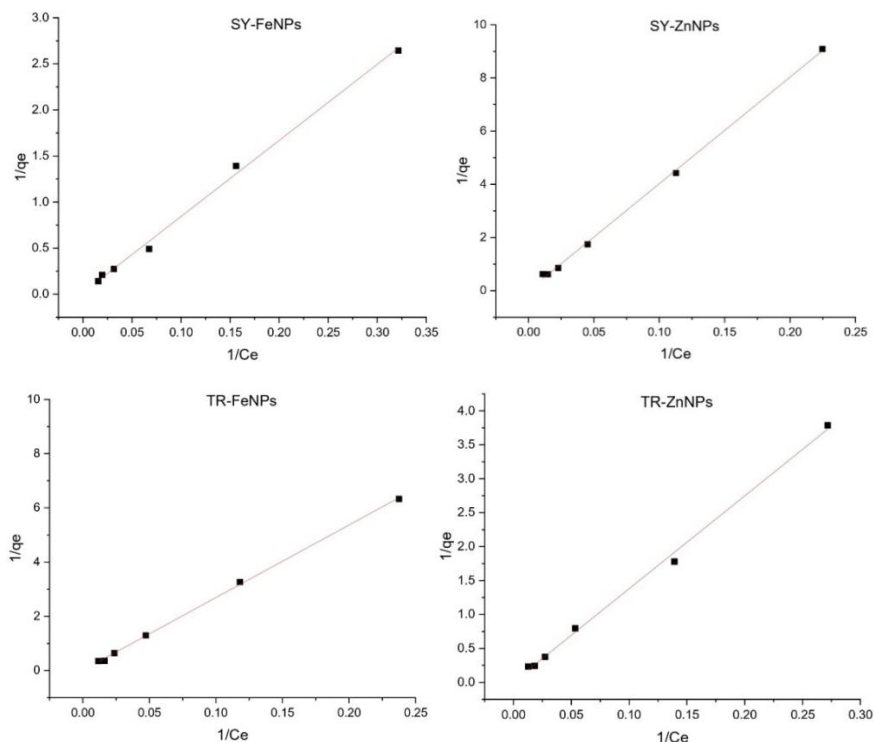


Fig. 7: Langmuir isotherm model for the reduction of sunset yellow and tartrazine using synthesized iron and zinc nanoparticles

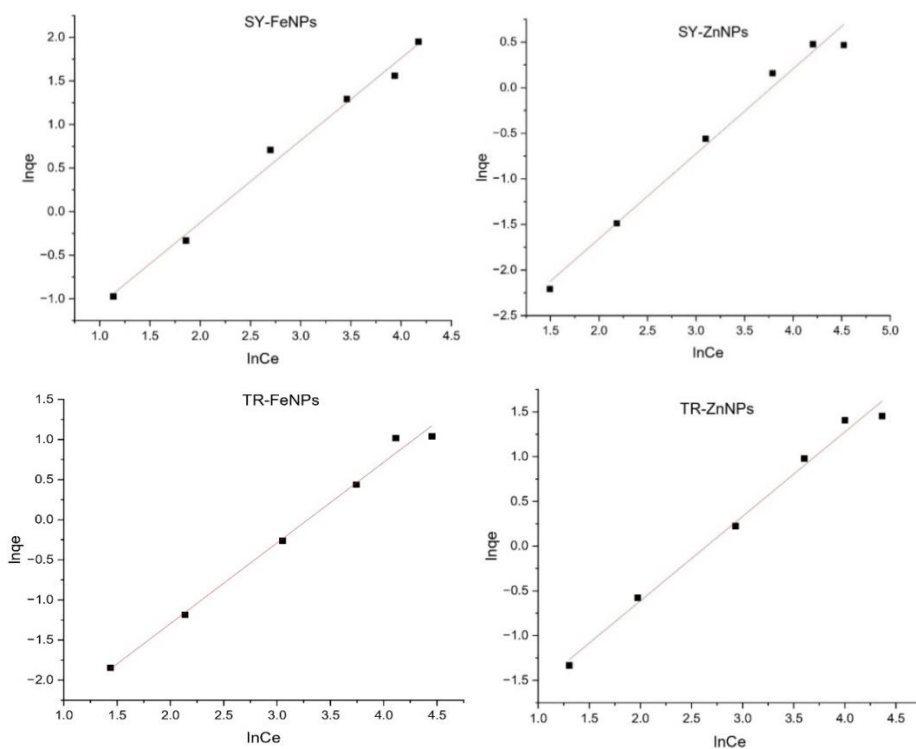


Fig. 8: Freundlich isotherm model for the reduction of sunset yellow and tartrazine using synthesized iron and zinc nanoparticles

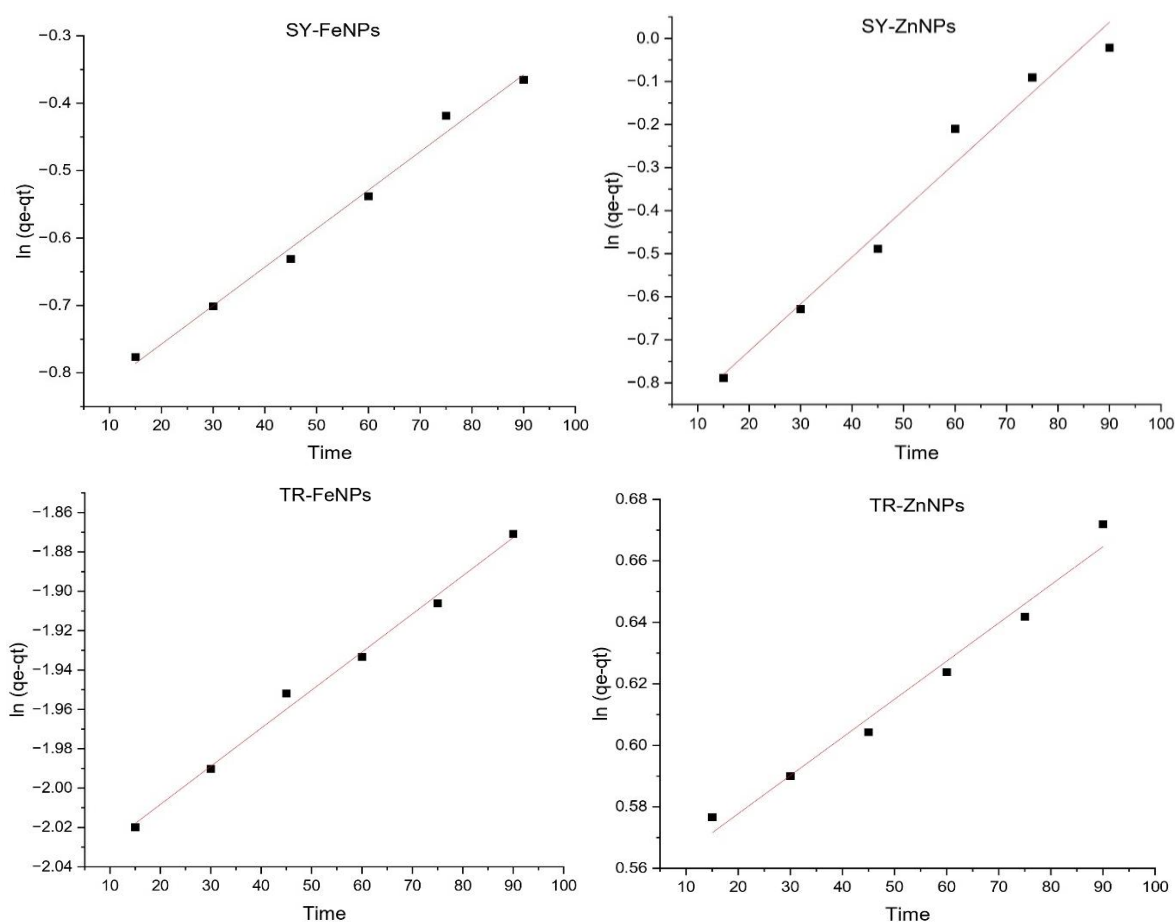
Table 1: Isotherm model parameters for the adsorption sunset yellow and tartrazine using synthesized iron and zinc nanoparticles

| S. No. | Equilibrium model | Parameter | Iron nanoparticles | | Zinc nanoparticles | |
|--------|-------------------|------------------|--------------------|------------|--------------------|------------|
| | | | Sunset yellow | Tartrazine | Sunset yellow | Tartrazine |
| 1 | Langmuir | q_{max} (mg/g) | 52.18 | 69.96 | 75.04 | 84.24 |
| | | K_L (L/mg) | 0.00232 | 0.00053 | 0.00033 | 0.00087 |
| | | R^2 | 0.9984 | 0.9996 | 0.9995 | 0.9986 |
| 2 | Freundlich | K_F (L/mg) | 1.0589 | 0.9942 | 1.0737 | 1.0596 |
| | | R^2 | 0.9955 | 0.9961 | 0.9926 | 0.9953 |

Kinetics of adsorption

The dye adsorption process using synthesized nanoparticles was evaluated using two different kinetic models i. e pseudo first order and pseudo second order models. The fitting results notably demonstrated a remarkable concurrence with the first-order model, as evidenced by the calculated correlation coefficient values. Furthermore, the application of the pseudo-first-order model yielded calculated adsorption capacities (q_e) that closely matched the experimental values (as displayed in table 4), showcasing a

perfect linear relationship across the entire range of dye concentrations. This exemplary fit to the first-order model suggests a kinetic mechanism in which both the dye ions and the adsorbent surface play essential roles, with the rate-determining step involving electron exchange between these two entities. The second order rate constant for the dye reduction study was noticed to be negative, suggests that the reaction doesn't follow second order and hence confirm that the adsorption follows pseudo-first order kinetics. The kinetic parameters were tabulated in table 2 and pseudo-first order kinetic plots were presented in fig. 9.

**Fig. 9: Pseudo-first order kinetic plots observed during the dye reduction study of synthesised nanoparticles****Table 2: Dye adsorption kinetic models of synthesized nanoparticles**

| S. No. | Kinetic order | Parameter | Iron nanoparticles | | Zinc nanoparticles | |
|--------|---------------|--------------|-----------------------|-----------------------|-----------------------|-----------------------|
| | | | Sunset yellow | Tartrazine | Sunset yellow | Tartrazine |
| 1 | First | K_1 | 6.34×10^{-5} | 2.15×10^{-5} | 1.21×10^{-4} | 1.38×10^{-5} |
| | | q_e (mg/g) | 2.626 | 0.472 | 0.926 | 1.825 |
| | | R^2 | 0.996 | 0.997 | 0.987 | 0.990 |
| 2 | Second | K_2 | -0.110 | -1.418 | -0.0468 | -0.064 |
| | | q_e (mg/g) | 2.626 | 0.472 | 0.926 | 1.825 |
| | | R^2 | 0.998 | 0.999 | 0.987 | 0.996 |

Stability and recyclability of nanoparticles

The chemical stability of the zinc nanoparticles synthesized in this study was evaluated across a pH range from 2.0 to 10. In the stability analysis, the metal content of the nanoparticles was compared to those synthesized in our study, and the percentage of stability was calculated. Fig. 10A illustrates that the synthesized nanoparticles maintained stability across the tested pH concentrations.

Assessing the reusability of the prepared nanoparticles was crucial for cost-effective analysis. In the initial cycle, the iron nanoparticles displayed impressive reusability rates of 98.59 ± 0.58 and 99.21 ± 0.37

% for the adsorption of sunset yellow and tartrazine, whereas the zinc nanoparticles exhibit 98.76 % and 98.45 % stability for the adsorption of sunset yellow and tartrazine respectively. As the cycles progressed, there was a slight decline in reusability, with rates of 95.81 ± 0.93 and 97.25 ± 0.87 % for the adsorption of sunset yellow and tartrazine whereas the zinc nanoparticles exhibit 95.23 ± 1.32 % and 94.32 ± 0.93 % observed at the fifth cycle (fig. 9B). This gradual decrease in efficiency may be attributed to the reduced availability of active sites within the nanoparticles due to the blockage of these sites by dye ions. In summary, the nanoparticles exhibited notable reusability with consistently high levels of adsorption efficiency.

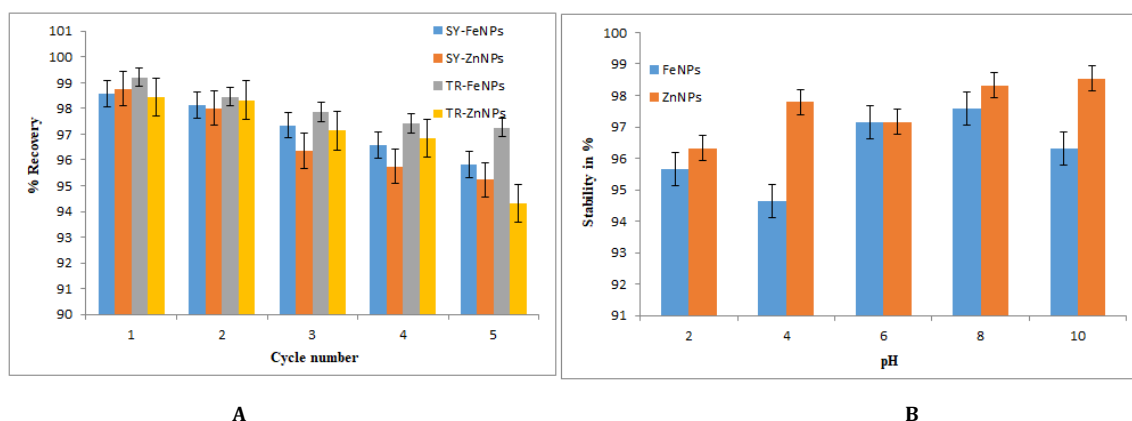


Fig. 10: Comparative stability and recyclability results of nanoparticles in the study, A) Stability of nanoparticles at various pH ranges; recyclability of nanoparticles B) Results presented in graph are the average of three replicate experiments

The outcomes obtained in this research were correlated with diverse adsorbents documented in the literature. In literature, Chukwuemeka *et al.*, 2021 [25] utilized *Cassava sievate* biomass derived nano carbon for the reduction of dyes and reported q_{max} of 22.40 mg/g and 30.06 mg/g, respectively for sunset yellow and tartrazine. Takdastan *et al.*, 2020 [26] reported q_{max} of 46.7 mg/g using persulfate-based magnetic Fe_3O_4 , Ghaedi *et al.*, 2012 [27] reported q_{max} of 19.94 mg/g using cadmium telluride nanoparticles loaded on activated carbon and Marzbani *et al.*, 2022 [28] studied commercial magnesium oxide nanoparticles and produce q_{max} of 1.55 mg/g for the reduction of sunset yellow dye. Zandipak *et al.*, 2016 [29] studied the effectiveness of $NiFe_2O_4$ nanoparticles fabricated using coprecipitation method for the reduction of sunset yellow and tartrazine and produce q_{max} value of 7.12 mg/g and 6.33 mg/g, respectively. The tartrazine reduction study conducted by Srivastava *et al.*, 2015 [30], Goscianska *et al.*, 2015 [31] and Rad *et al.*, 2020 [32] using various nanoparticles and reported q_{max} value of 32.60 mg/g, 27.18 mg/g and 19.81 mg/g respectively. The reported values were in correlation with the findings achieved in this study and confirm that the nanoparticles produced in this study exhibit effectiveness as an adsorbent for the removal of the investigated dyes.

CONCLUSION

This study presents the potential application of *Diospyros chloroxylon* (Roxb.), biogenically synthesized iron and zinc oxide nanoparticles as a highly effective nano-adsorbent for the decontamination of carcinogenic dyes such as sunset yellow and tartrazine. The study investigates the impact of various factors, including pH, contact time, temperature, and adsorbent dosage, on the removal of dyes and dyes, and these parameters are optimized for the process. Notably, the adsorption isotherms of iron and zinc nanoparticles for both dyes are found to be best described by the Langmuir model with maximum adsorption capacities. Hence, the nanoparticles synthesized in this study can exhibit outstanding adsorption and regenerative capabilities, making them a promising and suitable solution for the removal of toxic carcinogenic pollutants in water.

FUNDING

Nil

AUTHORS CONTRIBUTIONS

All the authors have contributed equally.

CONFLICT OF INTERESTS

Declared none

REFERENCES

- Bulgariu L, Escudero LB, Bello OS, Iqbal M, Nisar J, Adegoke KA. The utilization of leaf-based adsorbents for dyes removal: a review. *J Mol Liq.* 2019;276:728-47. doi: 10.1016/j.molliq.2018.12.001.
- Prabhu SM, Khan A, Hasmath Farzana M, Hwang GC, Lee Woojin, Lee G. Synthesis and characterization of graphene oxide-doped nano-hydroxyapatite and its adsorption performance of toxic diazo dyes from aqueous solution. *J Mol Liq.* 2018;269:746-54. doi: 10.1016/j.molliq.2018.08.044.
- Gomez M, Arancibia V, Rojas C, Nagles E. Adsorptive stripping voltammetric determination of tartrazine and sunset yellow in gelatins and soft drink powder in the presence of cetyl pyridinium bromide. *Int J Electrochem Sci.* 2012;7(8):7493-502. doi: 10.1016/S1452-3981(23)15799-3.
- Alves SP, Brum DM, Branco de Andrade EC, Pereira Netto AD. Determination of synthetic dyes in selected foodstuffs by high-performance liquid chromatography with UV-DAD detection. *Food Chem.* 2008;107(1):489-96. doi: 10.1016/j.foodchem.2007.07.054.
- Chung KT, Cerniglia CE. Mutagenicity of azo dyes: structure-activity relationships. *Mutat Res.* 1992;277(3):201-20. doi: 10.1016/0165-1110(92)90044-A, PMID 1381050.
- Konstantinou IK, Albanis TA. TiO_2 -assisted photocatalytic degradation of azo dyes in aqueous solution: kinetic and mechanistic investigations. *Appl Catal B.* 2004;49(1):1-14. doi: 10.1016/j.apcatb.2003.11.010.
- Subramani A, Jacangelo JG. Emerging desalination technologies for water treatment: a critical review. *Water Res.* 2015 May 15;75:164-87. doi: 10.1016/j.watres.2015.02.032, PMID 25770440.
- Ali I, AL-Othman ZA, Alwarthan A. Molecular uptake of congo red dye from water on iron composite nano particles. *J Mol Liq.* 2016 Dec 1;224:171-6. doi: 10.1016/j.molliq.2016.09.108.

9. Oturan MA, Aaron JJ. Advanced oxidation processes in water/wastewater treatment: principles and applications. A review. *Critical Reviews in Environmental Science and Technology*. 2014 Dec 2;44(23):2577-641. doi: 10.1080/10643389.2013.829765.
10. Robinson T, McMullan G, Marchant R, Nigam P. Remediation of dyes in textile effluent: a critical review on current treatment technologies with a proposed alternative. *Bioresour Technol*. 2001 May 1;77(3):247-55. doi: 10.1016/S0960-8524(00)00080-8, PMID 11272011.
11. Gupta VK, Suhas. Application of low-cost adsorbents for dye removal-a review. *J Environ Manage*. 2009;90(8):2313-42. doi: 10.1016/j.jenvman.2008.11.017. PMID 19264388.
12. Gupta M. Inorganic nanoparticles: an alternative therapy to combat drug-resistant infections. *Int J Pharm Pharm Sci*. 2021 Aug;13(8):20-31. doi: 10.22159/ijpps.2021v13i8.42643.
13. Huang L, Weng X, Chen Z, Megharaj M, Naidu R. Green synthesis of iron nanoparticles by various tea extracts: a comparative study of the reactivity. *Spectrochim Acta A Mol Biomol Spectrosc*. 2014 Sep 15;130:295-301. doi: 10.1016/j.saa.2014.04.037, PMID 24793479.
14. Ghosh MK, Sahu S, Gupta I, Ghorai TK. Green synthesis of copper nanoparticles from an extract of *Jatropha curcas* leaves: characterization, optical properties, CT-DNA binding and photocatalytic activity. *RSC Adv*. 2020;10(37):22027-35. doi: 10.1039/D0RA03186K, PMID 35516624.
15. Tulasi SL. Impact of zinc oxide nanoparticles on *Cajanus Cajan* Linn. with special reference to germination, vegetative and biochemical aspects. *JMPAS* 2023;12(1):5624-9. doi: 10.55522/jmpas.V12I1.4573.
16. Hoag GE, Collins JB, Holcomb JL, Hoag JR, Nadagouda MN, Varma RS. Degradation of bromothymol blue by 'greener' nano-scale zero-valent iron synthesized using tea polyphenols. *J Mater Chem*. 2009;19(45):8671-7, doi: 10.1039/B909148C.
17. Shahwan T, Sirriah AS, Nairat M, Boyac E, Eroglu AE, Scott TB, Hallam KR. Green synthesis of iron nanoparticles and their application as a fenton-like catalyst for the degradation of aqueous cationic and anionic dyes. *Chem Eng J*. 2011;172(1):258-66. <https://doi.org/10.1016/j.cej.2011.05.103>.
18. Tyagi PK, Gupta S, Tyagi S, Kumar M, Pandiselvam R, Daştan SD. Green synthesis of iron nanoparticles from spinach leaf and banana peel aqueous extracts and evaluation of antibacterial potential. *J Nanomater*. 2021;2021:1-11. doi: 10.1155/2021/4871453.
19. Alagiri M, Hamid SBA. Green synthesis of α -Fe₂O₃ nanoparticles for photocatalytic application. *J Mater Sci: Mater Electron*. 2014;25(8):3572-7. doi: 10.1007/s10854-014-2058-0.
20. Dana E, Taha A, Afkar E. Green synthesis of iron nanoparticles by *Acacia nilotica* pods extract and its catalytic, adsorption, and antibacterial activities. *Appl Sci*. 2018;8(10):1922/2076. doi: 10.3390/app8101922.
21. Pai S, HS, Varadavenkatesan T, Vinayagam R, Selvaraj R. Photocatalytic zinc oxide nanoparticles synthesis using peltophorum pterocarpum leaf extract and their characterization. *Optik*. 2019;185:248-55. doi: 10.1016/j.ijleo.2019.03.101.
22. Tulasi SL, Swamy AVVS, Pavani P, Subhashini V. Green synthesis of nanostructured zinc particles using aqueous leaf extract of *Schrebera swietenoides* roxb. and their catalytic application in the degradation of methyl orange, crystal violet dyes and chromium metal. *Int J App Pharm*. 2022;14(2):308-14. doi: 10.22159/ijap.2022v14i2.43697.
23. Gurgur E, Oluyamo SS, Adetuyi AO, Omotunde OI, Okoronkwo AE. Green synthesis of zinc oxide nanoparticles and zinc oxide-silver, zinc oxide-copper nanocomposites using *Bridelia ferruginea* as biotemplate. *SN Appl Sci*. 2020;2(5):911. doi: 10.1007/s42452-020-2269-3.
24. Nidhin M, Indumathy R, Sreeram KJ, Nair BU. Synthesis of iron oxide nanoparticles of narrow size distribution on polysaccharide templates. *Bull Mater Sci*. 2008 Feb;31(1):93-6. doi: 10.1007/s12034-008-0016-2.
25. Chukwuemeka Okorie HO, Ekuma FK, Akpomie KG, Nnaji JC, Okereafor AG. Adsorption of tartrazine and sunset yellow anionic dyes onto activated carbon derived from cassava sieveate biomass. *Appl Water Sci*. 2021 Feb;11(2):1-8. doi: 10.1007/s13201-021-01357-w.
26. Takdastan A, Pourfadakari S, Yousefi N, Oroojie N. Removal of sunset yellow dye using heterogeneous catalytic degradation with magnetic Fe₃O₄/persulfate/ultrasound system. *Desalin Water Treat*. 2020 Sep 1;197:402-12. doi: 10.5004/dwt.2020.25956.
27. Ghaedi M, Hekmati Jah AH, Khodadoust S, Sahraei R, Daneshfar A, Mihandoost A. Cadmium telluride nanoparticles loaded on activated carbon as adsorbent for removal of sunset yellow. *Spectrochim Acta A Mol Biomol Spectrosc*. 2012 May 1;90:22-7. doi: 10.1016/j.saa.2011.12.064, PMID 22306446.
28. Marzbani T, Khayatian G. Application of magnesium oxide nanoparticles for sunset yellow removal in aqueous solutions: adsorption isotherm, kinetic, and thermodynamic studies. *Iran J Chem Chem Eng*. 2022 May 22;41(12):3939-49. <https://doi.org/10.30492/IJCCE.2022.529057.4696>
29. Zandipak R, Sobhanardakani S. Synthesis of NiFe₂O₄ nanoparticles for removal of anionic dyes from aqueous solution. *Desalin Water Treat*. 2016 May 20;57(24):11348-60. doi: 10.1080/19443994.2015.1050701.
30. Srivastava V, Maydannik P, Sharma YC, Sillanpää M. Synthesis and application of polypyrrole coated tenorite nanoparticles (PPy@TN) for the removal of the anionic food dye 'tartrazine' and divalent metallic ions viz. Pb(ii), Cd(ii), Zn(ii), Co(ii), Mn(ii) from synthetic wastewater *RSC Adv*. 2015;5(98):80829-43. doi: 10.1039/C5RA14108G.
31. Goscianska J, Pietrzak R. Removal of tartrazine from aqueous solution by carbon nanotubes decorated with silver nanoparticles. *Catal Today*. 2015 Jul 1;249:259-64. doi: 10.1016/j.cattod.2014.11.017.
32. Jafari Rad A. Synthesis of copper oxide nanoparticles on activated carbon for pollutant removal in tartrazine structure. *JCC* 2020;2(3):99-104. doi: 10.29252/jcc.2.2.6.